

Dynamical Exchanges in Facilitated Models of Supercooled liquids

YounJoon Jung,¹ Juan P. Garrahan,² and David Chandler¹

¹*Department of Chemistry, University of California, Berkeley, CA 94720-1460*

²*School of Physics and Astronomy, University of Nottingham, Nottingham, NG7 2RD, UK*

(Dated: May 24, 2019)

We investigate statistics of dynamical exchange events in coarse-grained models of supercooled liquids in spatial dimensions $d = 1, 2$, and 3 . The models, based upon the concept of dynamical facilitation, capture generic features of statistics of exchange times and persistence times. Here, distributions for both times are related, and calculated for cases of strong and fragile glass formers over a range of temperatures. Exchange time distributions are shown to be particularly sensitive to the model parameters and dimensions, and exhibit more structured and richer behavior than persistence time distributions. Mean exchange times are shown to be Arrhenius, regardless of models and spatial dimensions. Specifically, $\langle t_x \rangle \sim c^{-2}$, with c being the excitation concentration. Different dynamical exchange processes are identified and characterized from the underlying trajectories. We discuss experimental possibilities to test some of our theoretical findings.

I. INTRODUCTION

Dynamical arrest of liquids as they approach the glass transition is a topic of much current research [1, 2, 3, 4]. This arrest entails such features as non-exponential relaxation and precipitous non-Arrhenius temperature dependence of transport properties. At its heart lies the notion of dynamic heterogeneity [5, 6, 7, 8, 9, 10, 11, 12]. Namely, as the temperature decreases towards the glass transition, mobility develops spatial inhomogeneity, and as time progresses local mobility undergoes dynamical changes. We have interpreted these phenomena [13, 14, 15, 16, 17] in terms of local excitations of mobility in space that propagate in time with facilitated dynamics [18, 19, 20, 21]. The excitations thus form lines in space-time. Dynamic scaling is described naturally in terms of the statistics of these lines [13, 14, 22, 23].

The work we present in this paper is motivated by recent experiments that directly detect local fluctuations of dynamics in supercooled liquids [7, 9, 11, 12, 24]. For example, single molecule rotational experiments [12] show that changes in local dynamics are similar to random telegraph noise, where local spatial regions exhibit dynamical exchanges between fast and slow dynamics. Similar stochastic behavior is also observed in local dielectric fluctuation experiments [7]. In those experiments a local spatial region exhibits dynamical exchanges between fast and slow dynamics, thus yielding direct confirmation of dynamic heterogeneity.

Considering these experiments, we establish generic features of statistical properties of dynamical exchange events and show how these features manifest themselves in experimental observables. In the low temperature regime, dynamics in supercooled liquids is dominated by fluctuations, not the mean. Therefore, it is pertinent to study the whole distribution in order to gain insights on the microscopic nature of dynamics in supercooled liquids and glasses.

We do so in this paper in the context of coarse-grained facilitated models. In Sec. II, we define these models.

In Sec. III, we define exchange and persistence times, and derive an analytical relationship between the distributions of exchange and persistence times. In Sec. IV, qualitative features of the exchange time distribution are presented. Numerical results of distributions of exchange and persistence times for the models are described in Sec. V. In Sec. VI we present results of numerical simulations of dynamic bleaching experiments. We conclude in Sec. VII with discussions of possible experimental measurements aimed at testing our theoretical predictions.

II. MODELS OF GLASS FORMERS

We assume that a kinetically constrained model [13, 14, 18, 20, 25] is obtained through coarse graining over a microscopic time scale δt (e.g., larger than the molecular vibrational time scale), and also over a microscopic length scale δl (e.g., larger than the equilibrium correlation length). The dimensionless Hamiltonian for the model is,

$$\mathcal{H} = \sum_{i=1}^N n_i, \quad (n_i = 0, 1). \quad (1)$$

Here, n_i refers to a state of lattice site i at \mathbf{x}_i , where $n_i = 1$ coincides with lattice site being a spatially unjammed region (i. e., carrying mobility), while $n_i = 0$ coincides with it being a jammed region (i. e., not carrying mobility). We thus call n_i the “mobility field”. In spatial dimensions $d = 1, 2$, and 3 , the lattice is linear, square, and cubic, respectively. The number of sites, N , specifies the size of the system. From Eq. (1), thermodynamics is trivial, and the equilibrium concentration of defects or excitations is given by

$$c = \langle n_i \rangle = \frac{1}{1 + \exp(1/T)}, \quad (2)$$

where T is a reduced temperature.

The dynamics of these models obey detailed balance with local dynamical rules that depend on the configuration of the lattice site i as well as those of its neighbors. Namely,

$$n_i(t) = 0 \xrightarrow{k_i^{(+)}} n_i(t + \delta t) = 1, \quad (3)$$

$$n_i(t) = 1 \xrightarrow{k_i^{(-)}} n_i(t + \delta t) = 0, \quad (4)$$

where

$$k_i^{(+)} = e^{-1/T} f_i(\{n_{\mathbf{x}}\}), \quad (5)$$

$$k_i^{(-)} = f_i(\{n_{\mathbf{x}}\}). \quad (6)$$

The function $f_i(\{n_{\mathbf{x}}\}) = f_i(n_1, n_2, \dots, n_N)$ reflects dynamical facilitation.

In the Fredrickson–Andersen (FA) model [18], a change of state at site i can occur from t to $t + \delta t$, $n_i(t + \delta t) = 1 - n_i(t)$, if at least one of $2d$ nearest neighbors of the i th site is excited. For example, in $d = 1$ case [18], $n_i(t + \delta t) = 1 - n_i(t)$ is allowed only if $n_j(t) = 1$ where $x_j = x_i \pm \delta l$. In contrast, in the $d = 1$ East model case [20], one needs an excited neighbor in specific directions in order to have a state change at site i . For instance, $n_j(t) = 1$ such that $x_j = x_i - \delta l$.

In $d = 3$ cases, $n_i(t)$ at $\mathbf{x}_i = (x, y, z)$ can make a change if at least there is one nearest neighbor site j such that $n_j(t) = 1$ at $\mathbf{x}_j = (x \pm \delta l, y, z)$ or $(x, y \pm \delta l, z)$ or $(x, y, z \pm \delta l)$ (FA model) or $\mathbf{x}_j = (x - \delta l, y, z)$ or $(x, y - \delta l, z)$ or $(x, y, z - \delta l)$ (East model). The facilitation function for the FA and East model, $f_i(\{n_{\mathbf{x}}\})$, is therefore given by,

$$[f_i(\{n_{\mathbf{x}}\})]_{\text{FA}} = 1 - \prod_{l=1}^d (1 - n_{\mathbf{x}_i + \delta l \hat{\mathbf{u}}_l})(1 - n_{\mathbf{x}_i - \delta l \hat{\mathbf{u}}_l}), \quad (7)$$

$$[f_i(\{n_{\mathbf{x}}\})]_{\text{East}} = 1 - \prod_{l=1}^d (1 - n_{\mathbf{x}_i - \delta l \hat{\mathbf{u}}_l}), \quad (8)$$

where $\hat{\mathbf{u}}_l$ is a unit vector in the l th dimension. In the classification scheme of kinetically constrained models given in Ref. [25], these kinetic constraints correspond to one-spin facilitation rule in d dimension.

III. EXCHANGE AND PERSISTENCE TIMES

Relaxation time scales of the glassy systems can be described by a distribution of *persistence times*, t_p , the time at which a local region changes its state for the first time once the trajectory has started at time zero. In the $d = 1$ FA model, for instance, the mean persistence time exhibits Arrhenius behavior at low temperatures [15].

A statistical measure which is useful in studying changes in dynamics of local environments is the distribution of *exchange times*, t_x , the time duration of given states of mobility fields. For example, it has been shown

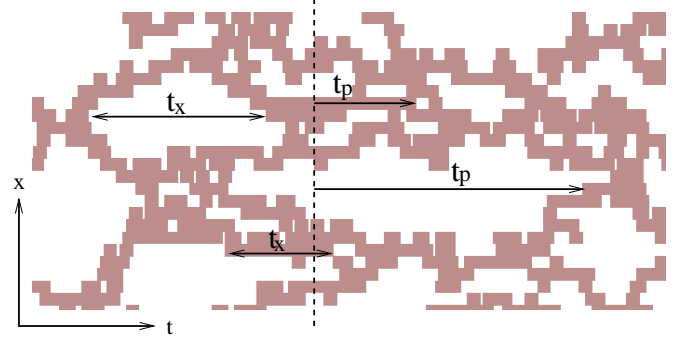


FIG. 1: Exchange and persistence times are shown in the trajectory of $d = 1$ FA model at $T = 0.8$. Shaded regions represent parts of space-time with excitations, while white regions represent parts with no excitations.

that the decoupling of the translational diffusion from the relaxation times in supercooled liquids near the glass transition can be explained from the distribution of exchange times [16, 17]. Persistence and exchange times are illustrated in the trajectory of $d = 1$ FA model in Fig. 1.

Exchange and persistence times are different statistical measures of the same trajectories. There is a general relation between exchange and persistence time distributions, independent of models. To derive the relation, we define the operator

$$P_i(t; 1, \tau) = \left[\prod_{t'=0}^{t-\delta t} n_i(\tau + t') \right] [1 - n_i(\tau + t)]. \quad (9)$$

It is the density of excitations at time τ (i.e., $n_i = 1$) that persist until time $t + \tau$. A similar expression for the density of unexcited sites that persist for this time frame, $P_i(t; 0, \tau)$, is given by Eq. (9) with n_i changed to $1 - n_i$, and $1 - n_i$ changed to n_i .

Similarly,

$$X_i(t; 1, \tau) = \frac{1}{\delta t} [1 - n_i(\tau - \delta t)] \left[\prod_{t'=0}^{t-\delta t} n_i(\tau + t') \right] \times [1 - n_i(\tau + t)], \quad (10)$$

is the density of excitations that exchange over the time interval between τ and $t + \tau$. Clearly,

$$X_i(t; 1, \tau) = \frac{1}{\delta t} [P_i(t; 1, \tau) - P_i(t + \delta t; 1, \tau - \delta t)]. \quad (11)$$

Averaging and taking $\delta t \rightarrow 0^+$ therefore yields

$$\mathcal{X}(t; 1) = -\frac{d\mathcal{P}(t; 1)}{dt}, \quad (12)$$

where $\mathcal{X}(t; 1) = \langle X_i(t; 1, \tau) \rangle$ and $\mathcal{P}(t; 1) = \langle P_i(t; 1, \tau) \rangle$. The normalized probability densities of exchange and persistence times for an excitation, $p_x(t; 1)$ and $p_p(t; 1)$,

respectively, are proportional to $\mathcal{X}(t; 1)$ and $\mathcal{P}(t; 1)$, respectively. Accounting for normalization constants therefore gives

$$p_p(t; 1) = \frac{\int_t^\infty dt' p_x(t'; 1)}{\langle t_x(1) \rangle}, \quad (13)$$

where $\langle t_x(1) \rangle = \int_0^\infty dt t p_x(t; 1)$ is the mean exchange time for an excitation.

One can also proceed the same route for persistence and exchange of no excitation by replacing n_i with $1 - n_i$ in Eqs. (9) and (10) to find

$$p_p(t; 0) = \frac{\int_t^\infty dt' p_x(t'; 0)}{\langle t_x(0) \rangle}. \quad (14)$$

The overall exchange and persistence time probability densities, $p_x(t)$, and $p_p(t)$, are given by

$$p_x(t) = \frac{1}{2} [p_x(t; 0) + p_x(t; 1)], \quad (15)$$

$$p_p(t) = (1 - c)p_p(t; 0) + cp_p(t; 1). \quad (16)$$

Using Eqs. (13) and (14) with the condition of detailed balance,

$$\frac{\langle t_x(1) \rangle}{\langle t_x(0) \rangle} = \frac{c}{1 - c}, \quad (17)$$

we find

$$p_p(t) = \frac{\int_t^\infty dt' p_x(t')}{\langle t_x \rangle}, \quad (18)$$

where $\langle t_x \rangle = \frac{1}{2}(\langle t_x(0) \rangle + \langle t_x(1) \rangle)$. For a Poisson process, which is valid for unconstrained dynamics, $p_x(t; n) = \tau(n)^{-1} \exp(-t/\tau(n))$. In that case, the exchange and persistence time distributions become identical to each other [26].

Moments of the two distributions are related to each other from Eq. (18) through integration by parts. In particular,

$$\langle (t_p)^m \rangle = \frac{\langle (t_x)^{m+1} \rangle}{(m+1)!\langle t_x \rangle}. \quad (19)$$

The moments of the persistence time distributions are always greater than those of the exchange time distributions when the distributions are broader than Poissonian. Correlations between exchange events are described by correlation functions of the type

$$C_{ij}(t, t' | n, \tau, n', \tau') = \langle \delta X_i(t; n, \tau) \delta X_j(t'; n', \tau') \rangle, \quad (20)$$

where $\delta X_i(t; n, \tau) \equiv X_i(t; n, \tau) - \mathcal{X}(t; n)$.

IV. ANALYSIS OF EXCHANGE TIME DISTRIBUTIONS

We have calculated exchange and persistence time distributions for the FA and East models by performing

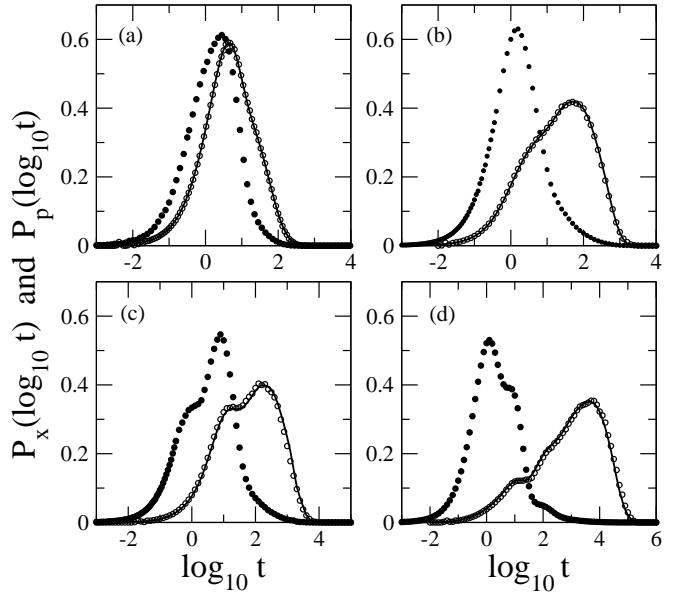


FIG. 2: Exchange and persistence time distributions for $d = 1$ FA and East models. Here, $P_x(\log_{10} t) = t p_x(t) \ln(10)$, and $P_p(\log_{10} t)$ is similarly related to $p_p(t)$. Exchange time distribution from simulation (filled circles), persistence time distribution from simulation (open circles), and persistence time distribution predicted from Eq. (18) (solid lines). (a) $d = 1$ FA model at $T = 1$, (b) $d = 1$ FA model at $T = 0.5$, (c) $d = 1$ East model at $T = 1$, and (d) $d = 1$ East model at $T = 0.5$.

Monte Carlo simulations. For the purpose of numerical efficiency, we have used the continuous time Monte Carlo algorithm [27, 28]. To sample long exchange times (i.e., $\log_{10} t_x > 1$), we have used $N = 100c^{-1}$. To sample short exchange times (i.e., $\log_{10} t_x < 1$), we have used $N = 10^5 c^{-1}$. The two distributions obtained were matched at $\log_{10} t_x = 1$. Simulations were performed for total times $\mathcal{T} = 500 \tau$, with τ being the relaxation time of the model. Averages were performed on about 100 independent trajectories in each case.

As an illustration, we show in Fig. 2 exchange and persistence time distributions obtained from numerical simulations, and compare those results with the prediction of Eq. (18). The comparison verifies Eq. (18). The peak and principal statistical weight in the persistence time distribution occurs at a longer time than that for the exchange time distribution.

A. Moments of Exchange and Persistence Times

In many experiments, measurements of moments of fluctuating quantities are more easily made than measurements of the whole distributions. Studies of moments will yield information on underlying dynamics [29, 30]. We have studied temperature dependence of the moments of exchange and persistence time distributions, $\langle (t_x)^m \rangle$ and $\langle (t_p)^m \rangle$ ($m=1, 2$, and 3), respectively, of the

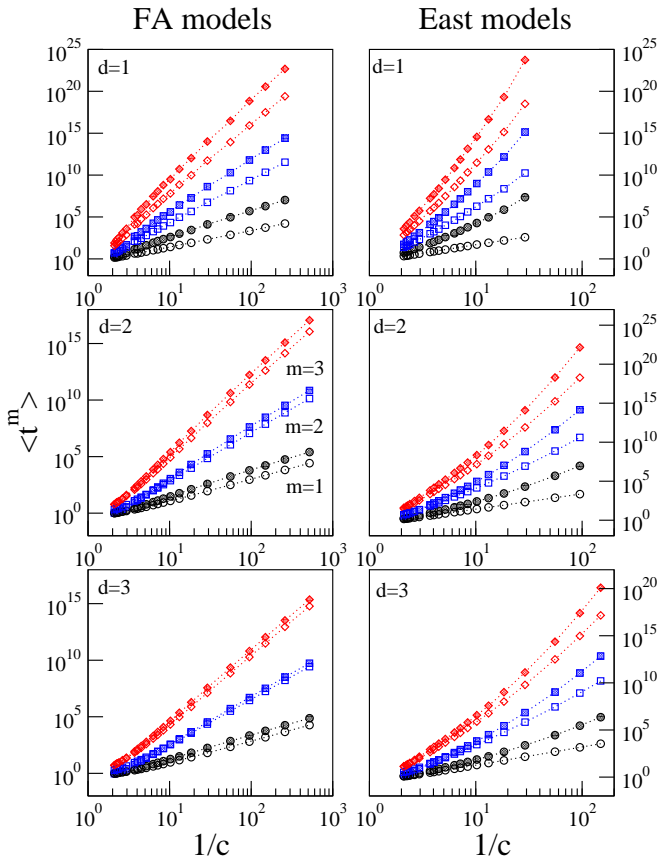


FIG. 3: The first (circles), second (squares), and third (diamonds) moments of exchange (open symbols) and persistence (shaded symbols) time distributions of $d = 1, 2$, and 3 FA models (left panels) and East models (right panels) as functions of excitation concentration, c .

FA and East models. Figure 3 shows these moments for dimensionality $d=1, 2$, and 3.

Moments of the exchange and persistence times reveal different temperature dependence for the FA and the East models. In the FA models, all the moments of exchange and persistence times increase in an Arrhenius fashion, $\langle t^m \rangle \sim c^{-\alpha_m}$, as the temperature (or the excitation concentration) decreases. In the East models only the mean exchange times are Arrhenius. Higher moments of exchange time distribution and all the moments of persistence time distribution in the East models are super-Arrhenius. Further, the mean persistence time is larger than the mean exchange time in all cases. Table I lists scaling exponents of the moments for the exchange and persistence times for Arrhenius cases.

We find that the mean exchange time increases approximately as

$$\langle t_x \rangle \sim c^{-2}, \quad (21)$$

in the low temperature limit in all cases, regardless of the models and dimensionality. To understand this result, we use Eqs. (7) and (8) to establish that the average value

FA models			East models
	$m = 1$	$m = 2$	$m = 3$
$d = 1$	2.0(3.2)	5.2(6.4)	8.4(9.7)
$d = 2$	1.9(2.3)	4.2(4.7)	6.6(7.0)
$d = 3$	1.9(2.1)	4.0(4.2)	6.1(6.3)

TABLE I: Scaling exponents for fitting various moments of exchange and persistence time distributions to Arrhenius form, $\langle t^m \rangle \sim c^{-\alpha_m}$ are shown for $d = 1, 2$, and 3 FA and East models. Numbers in the parenthesis are those for persistence time distributions. Fitting of the moments to the Arrhenius form was done for data corresponding to $T \leq 1$.

of facilitation function, $\langle f_i \rangle$, is

$$\langle f_i \rangle = 1 - (1 - c)^{ad}, \quad (22)$$

where $a = 2$ and 1 for FA and East models, respectively. As such, the mean exchange times for $n = 0$ and $n = 1$ states obtained from flip rates in Eqs. (5) and (6) are

$$\langle t_x(0) \rangle \approx 1/\langle k_i^{(+)} \rangle = \exp(1/T)/\langle f_i \rangle, \quad (23)$$

$$\langle t_x(1) \rangle \approx 1/\langle k_i^{(-)} \rangle = 1/\langle f_i \rangle, \quad (24)$$

and the overall mean exchange time, $\langle t_x \rangle = \frac{1}{2}(\langle t_x(0) \rangle + \langle t_x(1) \rangle)$, is

$$\langle t_x \rangle \approx \frac{1}{2c\langle f_i \rangle} = 12c[1 - (1 - c)^{ad}] \rightarrow \frac{1}{2adc^2}, \text{ as } c \rightarrow 0, \quad (25)$$

which shows the observed scaling of $\langle t_x \rangle \sim c^{-2}$ in the low temperature limit with a proportionality constant that depends on the dimensionality and model. Figure 4 shows that both the scaling and the proportionality constant predicted within Eq. (25) agree with the simulation results.

This behavior of the mean exchange time versus the excitation concentration has at least two experimental implications. First, experimental measurements that are insensitive to fluctuations of exchange times will not distinguish between fragile and strong glass formers. In order to distinguish, measurements of higher moments, or perhaps, the whole distributions will be required. The distribution could possibly be observed through single molecule experiments [12, 29, 30]. Second, the universal temperature dependence of the mean exchange time can form a basis of experimental measurements of excitation concentrations in real systems. The specific c^{-2} scaling holds to the extent that experimental systems can be modeled with single spin-flip facilitation rules.

In contrast to the behavior of the mean exchange time, the temperature dependence of mean persistence time, $\langle t_p \rangle$, depends on the model and the dimensionality. Relaxation times of the models are given by their mean persistence times, or from Eq. (19), the second moment of the exchange times. Temperature dependence of moments of exchange and persistence times shows that

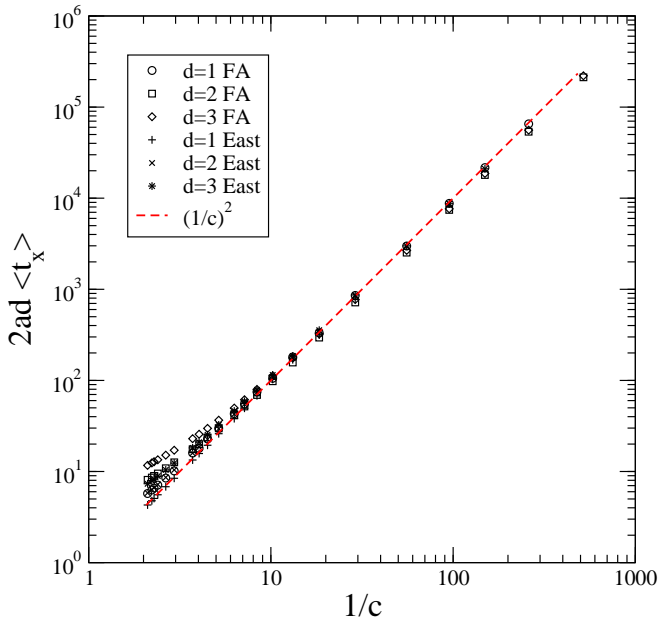


FIG. 4: Comparison of mean-field approximation, Eq. (25) (dashed line), and simulation results of mean exchange times in $d = 1, 2$, and 3 FA and East models. $a = 2$ for FA models and $a = 1$ for East models.

relaxation times are Arrhenius for the FA models and super-Arrhenius for the East models.

As the dimensionality of the model increases, differences between the moments of exchange and persistence times become smaller in the FA model. The model becomes increasingly mean-field like in higher dimensions. No such convergence is found in the East model for all dimensions investigated. The East models have weak dimensional dependence due to the quasi-one dimensional nature of directional persistence.

B. Stokes–Einstein Breakdown

In the FA models corresponding to strong glass formers, it was shown that in all dimensions the translational diffusion constant scales as [16]

$$D_{\text{FA}} \sim \langle t_x \rangle^{-1} \sim c^2. \quad (26)$$

According to this result, each exchange event can be considered separately, so that the number of diffusive steps are proportional to inverse of the mean exchange time. This is a good approximation in the FA models [16] because the excitation lines in the FA models perform diffusive dynamics.

But this picture breaks down in the case of hierarchical dynamics, where exchange events are correlated, as in the East models. In that case, higher moments of exchange time distributions exhibit different temperature dependence from that of the mean. This behavior is illustrated in Fig. 3 for the East model, which corresponds

to a fragile liquid. Correlations between successive exchange events can be investigated by using correlation function given in Eq. (20). The effects are responsible for non-trivial scaling relation between the translational diffusion and persistence times in fragile liquids [16, 31].

Indeed, numerical results for the fractional Stokes–Einstein relationship,

$$D \propto \tau_{\alpha}^{-\xi} \quad (27)$$

give $\xi \approx 2/3, 2/2.3, 2/2.1$ for dimensions $d = 1, 2, 3$ in the case of the FA models, while $\xi \approx 0.7 – 0.8$ (very weakly dependent on d) in the case of the East models [16, 31].

C. Classifications of Exchange Events

We show in Fig. 5 representative exchange time distributions. At short exchange times, $\log_{10} t_x < -1$, the distribution $P_x(\log_{10} t_x)$ follows a power-law behavior with a slope 1 in all cases, $P_x(\log_{10} t_x) \sim \log_{10} t_x$. This is because $P_x(\log_{10} t_x) \sim t_x p_x(t_x)$, and Poissonian statistics is obeyed, $p_x(t_x) \sim \exp(-t_x)$, for short times.

Multiple peak structures develop in the exchange time distributions at low temperature. In order to investigate the structure of exchange time distributions in detail, we define *mobility index*, $m_i(t)$, that depends upon whether the lattice site is filled with an excitation or not and also whether it is in a mobile or immobile configuration. Specifically,

$$m_i(t) = 4 - 2n_i(t) - f_i(t), \quad (28)$$

where $f_i(t) = 1$ when the lattice site i is in a mobile configuration at time t , and it is zero otherwise. As such, $m_i(t)$ is 1 when site i is excited and mobile, 2 when it is excited and immobile, 3 when it is unexcited and mobile, and 4 when it is unexcited and immobile.

During an exchange time of the lattice site i , n_i does not change, while its nearest neighbors may make flipping events, thus changing m_i over time. In order to monitor changes in the local mobility during an exchange time, it is useful to introduce an averaged mobility index for a single exchange event,

$$\bar{m}_i(t_s) = \frac{1}{t_x} \int_0^{t_x} dt' m_i(t_s + t'), \quad (29)$$

where t_s is the start time of an exchange event for site i , and the zero time in this formula is the time at which the exchange event begins. See Fig. 1. If there has not been any change in the local configuration during an exchange time, the lattice site remains always mobile, and the averaged mobility index will be either $\bar{m}_i = 1$ (for $n_i = 1$) or $\bar{m}_i = 3$ (for $n_i = 0$). However, when the local mobility changes during the exchange time period due to changes of the states in nearest neighbors, the averaged mobility index will be either $1 < \bar{m}_i < 2$ (for $n_i = 1$) or

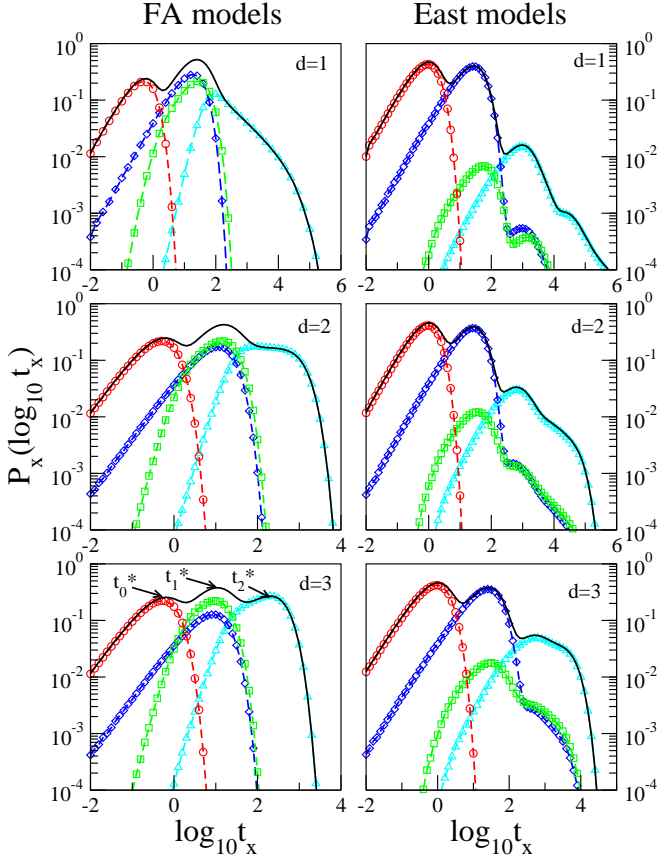


FIG. 5: Decompositions of exchange time distributions of FA models (left panels) and East models (right panels) for $d = 1, 2$, and 3 at $T = 0.3$. Four sub-distributions – case 1 (circles), case 2 (squares), case 3 (diamonds), and case 4 (triangles) – add up to the full distribution (solid line). Positions of three peaks in $P(\log_{10} t_x)$ are shown for $d = 3$ FA model cases.

$3 < \bar{m}_i < 4$ (for $n_i = 0$). We define four different cases of the averaged mobility. Namely,

- case 1 : $\bar{m}_i = 1$ ($n_i = 1$ and $f_i = 1$)
- case 2 : $1 < \bar{m}_i < 2$ ($n_i = 1$ and f_i changes)
- case 3 : $\bar{m}_i = 3$ ($n_i = 0$ and $f_i = 1$)
- case 4 : $3 < \bar{m}_i < 4$ ($n_i = 0$ and f_i changes).

Examples of exchange times that belong to each case are shown in the trajectory picture of $d = 1$ FA model in Fig. 6.

To illustrate the correlation between exchange times and environments, Fig. 5 shows exchange time distributions and their sub-distributions, each corresponding to one of the cases in Eq. (30), for $d = 1, 2$, and 3 FA and East models at $T = 0.3$. There exist multiple peaks in the distributions of exchange times at low temperature in all the cases shown in Fig. 5. Positions of peaks in the distribution, t_0^* , t_1^* , and t_2^* , are shown in the case of $d = 3$ FA model. Temperature dependence of these peaks for $d = 1, 2$, and 3 FA and East models are pre-

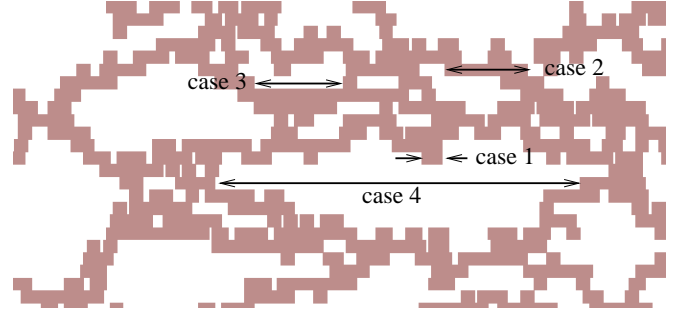


FIG. 6: Examples of exchange events that belong to each case of Eq. (30) are illustrated in the trajectory of $d = 1$ FA model.

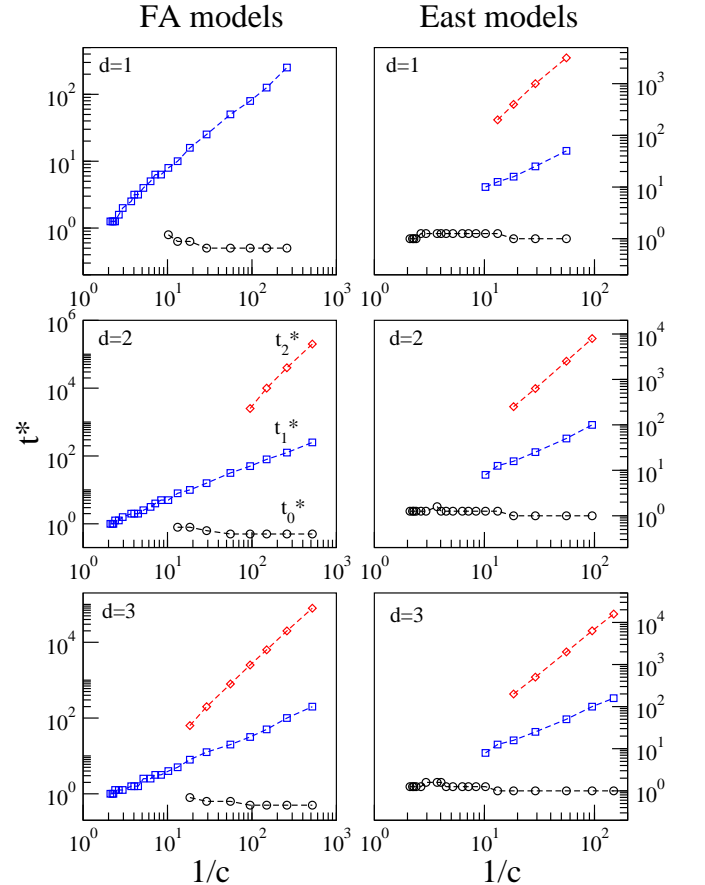


FIG. 7: Positions of peaks in the exchange time distributions are shown for various excitation concentrations.

sented in Fig. 7, and in all the cases, each peak position is Arrhenius,

$$t_n^* \sim c^{-n} \quad (31)$$

where $n = 0, 1$, and 2 .

To reveal the physical origins of each peak in the exchange time distributions, the temperature dependence of each peak in the exchange time distribution is shown

in Fig. 7. Cases 1 and 2 will involve disappearances of excitations, while cases 3 and 4 appearances of excitations in the trajectory space. The first peak in the exchange time distribution corresponds to fast processes of mobile $n = 1$ states embedded in the excitation line. In this case, the excited state will quickly de-excite in time $t_0^* \sim c^0$, and the position of the first peak in the exchange time distribution does not depend on the temperature as shown in Fig. 7. This process will have the averaged mobility index, $\bar{m} = 1$, corresponding to case 1 in Eq. (30).

The mobile region located at the boundary of excitation line will have a probability of becoming immobile due to changes in its nearest neighbors and becoming mobile later. This process corresponds to case 2 with the averaged mobility index $1 < \bar{m} < 2$. It is responsible for fluctuations of thicknesses of excitation lines in trajectory space, and it gives rise to the second peak in the exchange time distribution, with temperature dependence $t_1^* \sim c^{-1}$.

Dynamical exchange processes corresponding to case 3 also contribute to the second peak in the distribution. In this case, $n = 0$ state next to an excitation line becomes excited in time $t_1^* \sim c^{-1}$. This process involves a creation of an excitation next to a pre-existing excitation line. In terms of the geometry of the trajectory space, exchange events corresponding to cases 2 and 3 are responsible for bending of excitation lines.

Finally, the exchange events that have the longest times, resulting in the third peak, will correspond to the up-flip event of the $n = 0$ states far away from the excitation lines. This case has the averaged mobility index of case 4. In $d = 1$ FA model, for example, it corresponds to a region deep inside the bubble structure in the trajectory space.

V. DISTRIBUTIONS OF EXCHANGE AND PERSISTENCE TIMES

A. Strong Glass Former Models

Figure 8 compares the exchange time distributions (left panels) and persistence time distributions (right panels) for $d = 1, 2$, and 3 FA models at various temperatures. Exchange time distributions shown in the left panel depend strongly on the temperature. In the high temperature regime, the exchange time distribution has a single peak because there is no clear distinction between different exchange events due to the mean-field nature of the dynamics in the high temperature regime. However, as temperature decreases, the mean-field picture is no longer valid, excitation lines dominate trajectory space, and different kinds of dynamical exchange events manifest themselves in the distribution as distinct peaks. This fact is evident from the multiple peak structures in the exchange time distribution in all dimensions in the FA model. In $d = 3$ FA model, for instance, distinct triplet structure is observed when $T = 0.4$ and below. Each peak

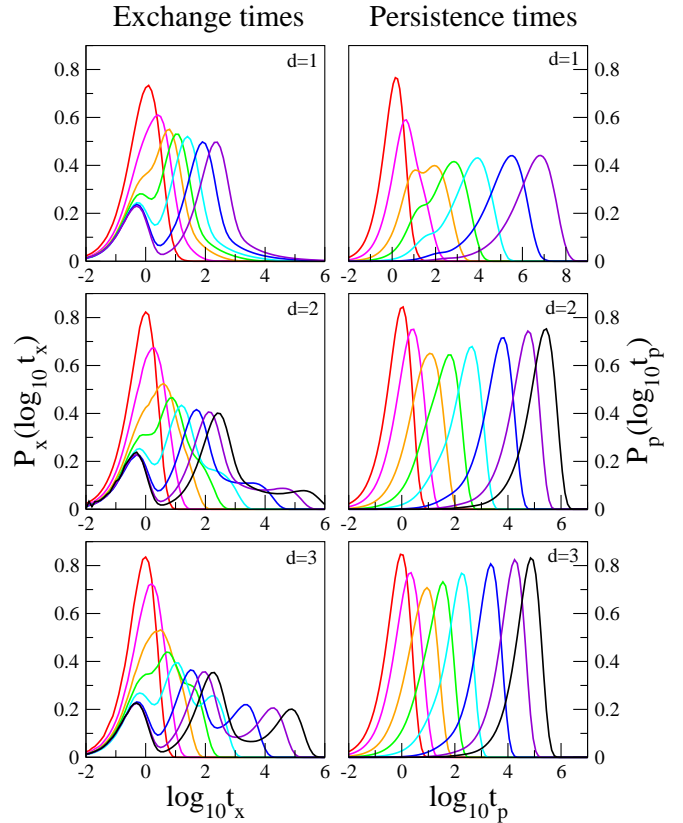


FIG. 8: Distributions of the logarithm of exchange and persistence times of FA model for $d = 1, 2$, and 3 at various temperatures. From left to the right: $T = 10, 1, 0.55, 0.4, 0.3, 0.22, 0.18$ for $d = 1$ case, and $T = 10, 1, 0.55, 0.4, 0.3, 0.22, 0.18, 0.16$ for $d = 2$ and $d = 3$ cases.

corresponding to different dynamical exchange event exhibits different behaviors of temperature dependence as presented in Fig. 7.

As the dimensionality increases, the exchange time distribution shows more and more well-separated triplet peak structure in the low temperature regime. The relative weight of the third peak increases as the dimensionality increases.

The persistence time distributions shown in the right panel of Fig. 8 are less structured than the exchange time distributions, as to be expected from Eq. (18). As the temperature decreases, the single peak in the persistence time distribution moves towards the long time region. Physically, persistence time distributions are statistical measures of duration of a state at an arbitrary space-time point in the trajectory space. Thus, relative to exchange time distributions, persistence time distributions emphasize processes occurring over longest times. The greater structure in the exchange time distributions, relative to the persistence time distributions, is due to the former giving equal weights to events, irrespective of their durations.

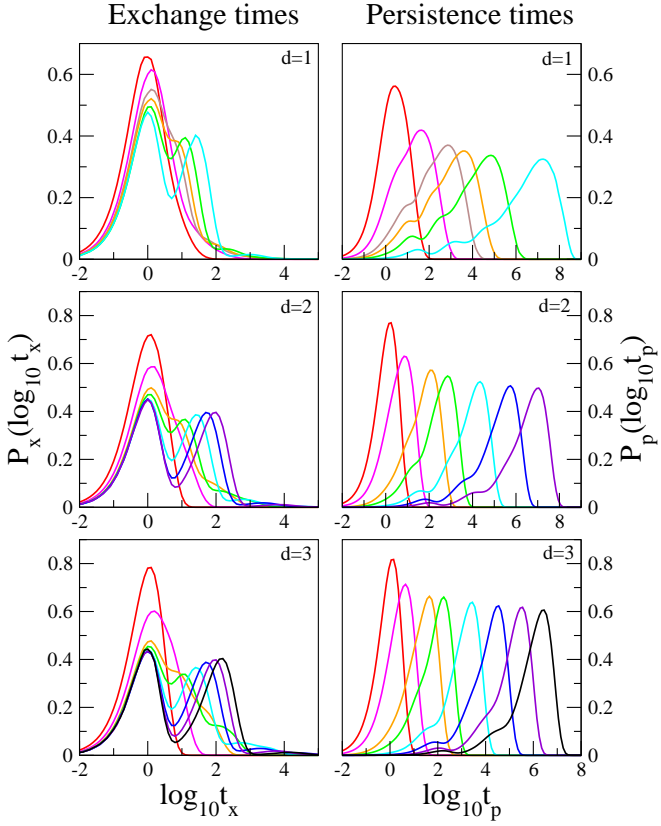


FIG. 9: Distributions of the logarithm of exchange and persistence times of East model for $d = 1, 2$, and 3 at various temperatures. From left to the right: $T = 10, 1, 0.6, 0.5, 0.4$, and 0.3 for $d = 1$ case, $T=10, 1, 0.5, 0.4, 0.3, 0.25$, and 0.22 for $d = 2$ case, and $T=10, 1, 0.5, 0.4, 0.3, 0.25, 0.22$, and 0.2 for $d = 3$ case.

B. Fragile Glass Former Models

Exchange and persistence time distributions for the East model cases are shown in Fig. 9. In the high temperature regime, the exchange time distributions have a single peak as in strong liquids or FA models. However, in the low temperature regime, in contrast with its behavior in the FA model, they show two dominant doublet peaks in all dimensions. We also notice that, albeit small, broad tails develop in the wings of the distributions at low temperatures. This feature is especially evident in Fig. 10, where the exchange time distributions of the FA and East models are compared in log–log scale. In the case of persistence time distributions shown in the right panel of Fig. 9, single peaks develop into broad distributions with shoulders as temperature decreases.

We compare exchange time distributions in FA and East models in Fig. 10. In $d = 1$ case, exchange time distributions of both FA and East models show long time tails in the low temperature regime in common. Additionally, the distributions in the East model exhibit logarithmic oscillations. In higher dimensions, $d = 2$ and

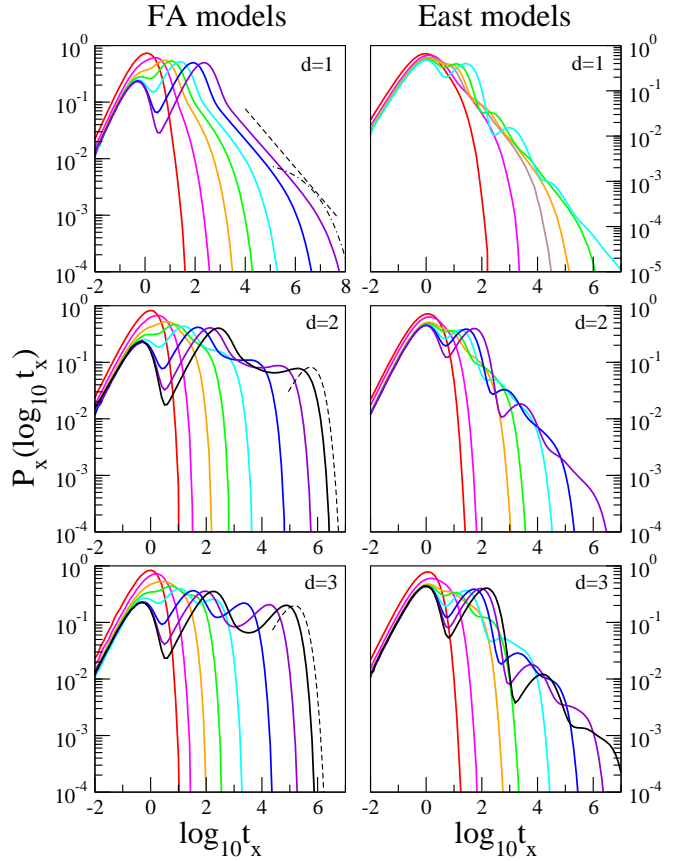


FIG. 10: Exchange time distributions of FA models (left panels) and East models (right panels) in log scales. Temperatures are the same as those given in the captions to Figs. 8 and 9. A power-law corresponding to $p_x(t_x) \sim t_x^{-\alpha}$ or $P_x(\log_{10} t_x) \sim t_x p_x(t_x) \sim t_x^{1-\alpha}$ is shown as a dashed line with $\alpha = 0.52$, and a stretched exponential corresponding to $p_x(t_x) \sim e^{-(t_x)^\beta}$ where $\beta = 0.38$ is shown as a dot-dashed line for $d = 1$ FA model. In $d = 2$ and 3 FA models, exponential fits, $p_x(t_x) \sim e^{-t_x/\tau}$, are given as dashed lines for the lowest temperature of each case.

3, the exchange time distributions in FA models exhibit distinct multiplet peak structures due to their mean-field natures in higher dimensions. However, the distributions in the East models remain similar to those in $d = 1$ cases, exhibiting long time tails and superimposed logarithmic oscillations. These are due to the hierarchical dynamics that arise from directed facilitation in the East models at all dimensions.

In the $d = 1$ FA case, due to the formations of bubble-like structures in the trajectory space, the exchange time distributions decay with slowly decaying long time tails. It turns out that in $d = 1$ FA model case the exchange time distribution first decays as a power-law (dashed line) then turns into a stretched exponential (dot-dashed line) as shown in Fig. 10. However, in $d = 2$ and $d = 3$ FA models, they decay as an exponential at the long time region shown as dashed lines. This indicates that in higher

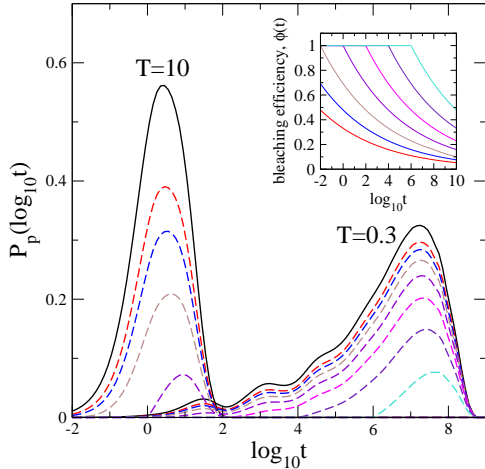


FIG. 11: Persistence time PDF's at a high ($T = 10$) and a low ($T = 0.3$) temperature at equilibrium (solid lines) and right after the bleaching (dotted lines). Each dashed line corresponds to the distribution created by bleaching efficiency function, $\phi(t)$ with different values of τ , given in the inset of Fig. (11). Inset: Bleaching efficiency function used in the simulation, Eq. (32), with $\alpha = 0.08$. From left to the right, τ progressively increases from $\tau = 10^{-6}$ to $\tau = 10^6$ by a factor of 100.

dimensions the FA models are less “glassy” than $d = 1$ case. In higher dimensions, chances of forming bubble-like structures will be much smaller than in $d = 1$ case. In the East model cases, similar behaviors are observed in all dimensions. Namely, the exchange time distributions decay with multiple transitions superimposed with stretched exponentials in the low temperature regime.

VI. SIMULATIONS OF BLEACHING EXPERIMENTS

Experiments have been performed in order to measure the timescale of the approach of non-equilibrium distributions of local relaxation times to equilibrium [9, 32, 33, 34]. The timescale at which the non-equilibrium distribution approaches to equilibrium will be called the *recovery time*. Based on the $d = 1$ East model, we present results of numerical simulations of one of such experiments - dynamical hole burning experiments or bleaching experiments [9, 32].

In numerical simulations of the bleaching experiment, the bleaching efficiency function, $\phi(t)$, is introduced as a probability of bleaching out the region that has a local persistence time of t . We choose the following form as $\phi(t)$,

$$\phi(t) = \min [1, (\tau/t)^\alpha], \quad (32)$$

where τ and α can be varied. We choose $\tau = 1$, and $\alpha = 0.08$ motivated by experimental results in [32]. After a lattice site is chosen to be “bleached out” in simulations,

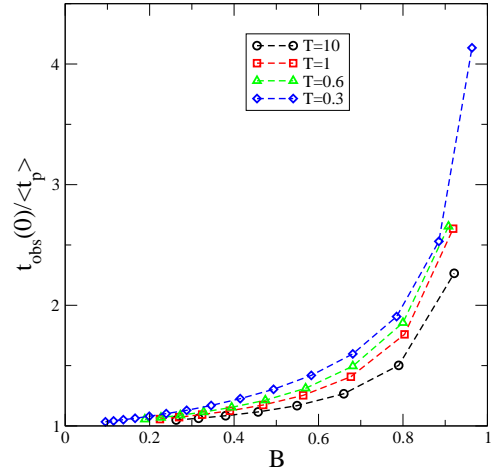


FIG. 12: Mean persistence times right after the bleaching experiment, $t_{\text{obs}}(0)$, are shown for various bleaching depths and temperatures. $t_{\text{obs}}(0)$ increases more abruptly as a function of the bleach depth at a lower temperature.

persistence times of that site are not collected at later times as time goes on.

Numerical values of the bleaching efficiency functions are shown in the inset of Fig. 11. The bleaching depth, B , is defined as the fraction of lattice sites that are bleached out by applying the bleaching efficiency function, and is given by

$$B = \int_0^\infty dt \phi(t) p_p(t). \quad (33)$$

Probability distributions of persistence times after the bleaching are shown in Fig. 11 for two different values of the temperature and various values of τ .

Immediately after the bleaching, the system is out of equilibrium, with a non-equilibrium persistence time distribution given (to within a normalization constant) by

$$p_{\text{ne}}(t) = \frac{p_p(t)(1 - \phi(t))}{1 - B}. \quad (34)$$

After waiting a time t_w , this distribution relaxes to $p(t; t_w)$, where $p(t; 0)$ is $p_{\text{ne}}(t)$ and $p(t; \infty)$ is the equilibrium $p_p(t)$. $t_{\text{obs}}(t_w)$ is the first moment of $p(t; t_w)$,

$$t_{\text{obs}}(t_w) = \int_0^\infty dt t p(t; t_w), \quad (35)$$

and $t_{\text{obs}}(0) > \langle t_p \rangle$. $t_{\text{obs}}(0)$ at various bleaching depths and temperatures are shown in Fig. 12.

The relaxation dynamics is monitored by following a time evolution of the non-equilibrium persistence time distribution obtained from unbleached lattice sites for various waiting times, t_w . Figure 13 shows the relaxation dynamics of the initial non-equilibrium distribution of persistence times for $d = 1$ East model at a low temperature.

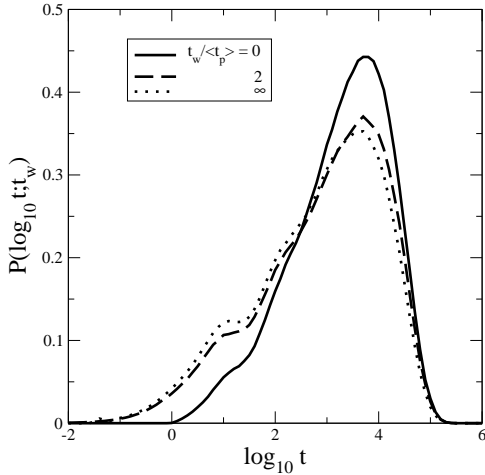


FIG. 13: Relaxation dynamics of the distributions of persistence times to equilibrium after the bleaching of $d = 1$ East model at $T = 0.5$. $\tau = 1$ and $\alpha = 0.08$ were chosen in $\phi(t)$.

The timescale of the relaxation process of the non-equilibrium distribution can be estimated by several means. For example, one can look at the waiting time dependence of moments of the distributions. Also, it is possible to measure how far a non-equilibrium distribution is separated from equilibrium by defining a distance between two distributions by

$$\Delta(t_w) \equiv \int_0^\infty dt |p(t; t_w) - p_p(t)|. \quad (36)$$

$\Delta(t_w)$ and the first three moments of the non-equilibrium distribution are shown in Fig. 14 for different values of the waiting time. From these calculations, the timescale of a recovery to equilibrium is estimated to be on the order of the equilibrium mean persistence time, $\langle t_p \rangle$. This predication is at variance with results from bleaching experiments [9, 32], but is consistent with results from NMR experiments [33, 34]. The reason(s) for this discrepancy remains to be clarified.

VII. DISCUSSION

Many theoretical predictions made in this work can be directly tested in experiments. First, it should be possible to test in experiments the relation between exchange and persistence time distributions given in Eq. (18) and the resulting relation between the moments of those distributions given in Eq. (19). This test requires detecting the full range of dynamical exchange events, ranging from fast to slow processes. Doing so with single molecule experiments [7, 12] will require probe molecules with long photo-bleaching times.

Second, once the distributions of exchange times are obtained, we are in a position to study temperature dependences of their moments. In particular, we have

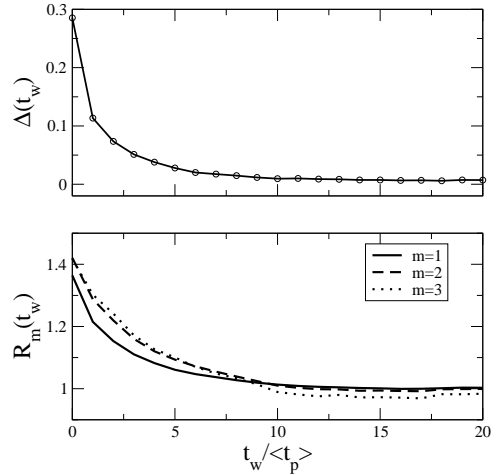


FIG. 14: Recovery of the non-equilibrium distribution, $p(t; t_w)$ to equilibrium is shown by the decay of $\Delta(t_w)$ (upper panel) and $R_m(t_w) \equiv \langle (t_{\text{obs}}(t_w))^m \rangle / \langle (t_p)^m \rangle$ (lower panel). Timescale of the recovery to equilibrium is on the order of the equilibrium mean persistence time itself. The model parameters are the same as those used in Fig. 13.

pointed out that the mean exchange time behaves always in an Arrhenius fashion, $\langle t_x \rangle \sim c^{-2}$, independent of the fragility and the dimensionality. This universal behavior of mean exchange times should be verified with ensemble measurements. Also, provided the proportionality between mean exchange time and excitation concentration is established, this relationship can be used to obtain the concentration of excitations in real glass formers, the key control parameter in our theory.

Third, higher moments of exchange time distributions obtained from single molecule experiments have information on fragility of supercooled liquids. While the first moment of exchange time distributions is always Arrhenius, higher moments show temperature dependences that are system dependent. For strong liquids, higher moments of exchange time distribution are Arrhenius, while for fragile liquids the higher moments are super-Arrhenius. Thus, one can make correlations between fragility of liquids and the temperature dependence of higher moments of exchange time distributions obtained from experiments.

Fourth, it is plausible to establish connections between seemingly different types of measurements of dynamical quantities in glass formers, such as translational diffusion constants [9, 35, 36, 37], and exchange time distributions [12]. We have shown that in the case of strong liquids mean exchange times can be used to estimate the translational diffusions constant, whereas in fragile liquids one needs to consider not only the mean but also correlations between exchange events and higher moments of exchange time distributions. Correlations between the Stokes-Einstein breakdown, higher moments of exchange time distributions, and fragility of liquids can be tested

by combining those two different types of experiments.

Finally, in many experiments, a probe molecule is usually introduced into a liquid as a local reporter of environmental changes. Inevitably, the size of the probe is important. For example, the Stokes-Einstein breakdown appears less significant in the case of larger probes than for smaller probes [37]. This probe-size dependence might be anticipated in terms of space-time scaling, and it merits further exploration.

Acknowledgment

We are grateful to M.D. Ediger, D.A. Vanden Bout, and A. Heuer for useful discussions. This work was sup-

ported at Berkeley by the Miller Research Institute for Basic Research in Sciences (YJ) and by the US Department of Energy Grant No. DE-FG03-87ER13793 (DC), and at Nottingham by EPSRC grants no. GR/R83712/01 and GR/S54074/01 and University of Nottingham grant no. FEF 3024 (JPG).

- [1] M. D. Ediger, C. Angell, and S. Nagel, *J. Phys. Chem.* **100**, 13200 (1996).
- [2] C. A. Angell, *Science* **267**, 1924 (1995).
- [3] P. G. Debenedetti and F. H. Stillinger, *Nature* **410**, 259 (2001).
- [4] W. Kob, in *Slow relaxations and nonequilibrium dynamics in condensed matter*, Eds. J.-L. Barrat and M. V. Feigel'mand and J. Kurchan and J. Dalibard (Springer Verlag, Berlin, 2003), p. 199, Les Houches Session LXVII, see also cond-mat/0212344.
- [5] For experimental evidences, see, for example, K. Schmidt-Rohr and H. Spiess, *Phys. Rev. Lett.* **66**, 3020 (1991); R. Richert, *Chem. Phys. Lett.* **199**, 355 (1992); M.T. Cicerone and M.D. Ediger, *J. Chem. Phys.* **103**, 5684 (1995); E. Weeks, J.C. Crocker, A.C. Levitt, A. Schofield, and D.A. Weitz, *Science* **287**, 627 (2000); W. K. Kegel and A. van Blaaderen, *Science* **287**, 290 (2000); E.R. Weeks and D.A. Weitz, *Phys. Rev. Lett.* **89**, 095704 (2002).
- [6] For numerical evidences, see, for example, T. Muranaka and Y. Hitawari, *Phys. Rev. E* **51**, R2735 (1995); D. Perera and P. Harrowell, *Phys. Rev. E* **51**, 314 (1995); R. Yamamoto and A. Onuki, *Phys. Rev. E* **58**, 3515 (1998). B. Doliwa and A. Heuer, *Phys. Rev. Lett.* **80**, 4915 (1998); C. Donati, J.F. Douglas, W. Kob, S.J. Plimpton, P.H. Poole and S.C. Glotzer, *Phys. Rev. E* **60**, 3107 (1999); C. Bennemann, C. Donati, J. Baschnagel and S.C. Glotzer, *Nature* **399**, 246 (1999). N. Lacevic, F.W. Starr, T.B. Schröder and S.C. Glotzer, *J. Chem. Phys.* **119**, 7372 (2003); M. Vogel and S.C. Glotzer, *Phys. Rev. Lett.* **92**, 255901 (2004).
- [7] E. Vidal Russell and N. E. Israeloff, *Nature* **408**, 695 (2000).
- [8] H. Sillescu, *J. Non-Cryst. Solids* **243**, 81 (1999).
- [9] M. D. Ediger, *Ann. Rev. Phys. Chem.* **51**, 99 (2000).
- [10] S. C. Glotzer, *J. Non-Cryst. Solids* **274**, 342 (2000).
- [11] R. Richert, *J. Phys.: Condens. Matter* **14**, R703 (2002).
- [12] L. A. Deschenes and D. A. vanden Bout, *Science* **292**, 255 (2001); *J. Phys. Chem. B* **106**, 11438 (2002).
- [13] J. P. Garrahan and D. Chandler, *Phys. Rev. Lett.* **89**, 035704 (2002).
- [14] J. P. Garrahan and D. Chandler, *Proc. Natl. Acad. Sci.* **100**, 9710 (2003).
- [15] L. Berthier and J. P. Garrahan, *Phys. Rev. E* **68**, 041201 (2003).
- [16] Y. Jung, J. P. Garrahan, and D. Chandler, *Phys. Rev. E* **69**, 061205 (2004).
- [17] L. Berthier, D. Chandler, and J. P. Garrahan, *Europhys. Lett.* **69**, 230 (2005).
- [18] G. H. Fredrickson and H. C. Andersen, *Phys. Rev. Lett.* **53**, 1244 (1984).
- [19] R. G. Palmer, D. L. Stein, E. Abrahams, and P. W. Anderson, *Phys. Rev. Lett.* **53**, 958 (1984).
- [20] J. Jäckle and S. Eisinger, *Z. Phys. B* **84**, 115 (1991).
- [21] S. Butler and P. Harrowell, *J. Chem. Phys.* **95**, 4454 (1991).
- [22] L. Berthier, *Phys. Rev. E* **69**, 020201 (2004).
- [23] S. Whitelam, L. Berthier, and J. P. Garrahan, *Phys. Rev. Lett.* **92**, 185705 (2004); *Phys. Rev. E.*, **71**, 026128 (2005).
- [24] A. P. Bartko, K. W. Xu, and R. M. Dickson, *Phys. Rev. Lett.* **89**, 026101 (2002).
- [25] F. Ritort and P. Sollich, *Adv. Phys.* **52**, 219 (2003).
- [26] In the context of the renewal theory exchange and persistence times are known as total and excess lifetimes, and the relation between probability density functions of the total and excess lifetimes is valid in the same way as that for the exchange and persistence times. See, for example, G. Grimmett and D. Stirzaker, *Probability and random processes*, 3rd. ed., Oxford University Press, 2001.
- [27] A. B. Bortz, M. H. Kalos, and J. L. Lebowitz, *J. Comp. Phys.* **17**, 10 (1975).
- [28] M. E. J. Newman and G. T. Barkema, *Monte Carlo Methods in Statistical Physics* (Oxford University Press, Oxford, 1999).
- [29] Y. Jung, E. Barkai, and R. J. Silbey, *Adv. Chem. Phys.* **123**, 199 (2002).
- [30] E. Barkai, Y. Jung, and R. J. Silbey, *Annu. Rev. Phys. Chem.* **55**, 457 (2004).
- [31] Y. Jung, J. P. Garrahan, and D. Chandler, unpublished (2005).
- [32] C.-Y. Wang and M. D. Ediger, *J. Phys. Chem. B* **103**, 4177 (1999).
- [33] K. Schmidt-Rohr and H. Spiess, *Phys. Rev. Lett.* **66**, 3020 (1991).
- [34] R. Bohmer, G. Hinze, G. Diezemann, B. Geil, and

H. Sillescu, *Europhys. Lett.* **36**, 55 (1996).

[35] F. Fujara, B. Geil, H. Sillescu, and G. Fleishcer, *Z. Phys. B* **88**, 195 (1992).

[36] I. Chang and H. Sillescu, *J. Phys. Chem. B* **101**, 8794 (1997).

[37] S. F. Swallen, P. A. Bonvallet, R. J. McMahon, and M. D. Ediger, *Phys. Rev. Lett.* **90**, 015901 (2003).